ACS OMEGA

http://pubs.acs.org/journal/acsodf

Article

Ionic Liquid Functionalized Metal−Organic Framework ([DEIm][PF_6]@MOF-5): Synthesis, Characterization, and Catalytic Application in the Reduction of 4-Nitrophenol

Abdulaziz Abdullah Qasem Ali and Zeba N. Siddiqui*

Cite This: *ACS Omega* 2023, 8, 3785−3797

Read Online

ACCESS | Metrics & More | Article Recommendations | Supporting Information

ABSTRACT: A novel, unique, highly effective, and recyclable heterogeneous catalyst, diethyl imidazolium hexafluorophosphate ionic liquid supported metal−organic framework ([DEIm][PF_6]@MOF-5), has been synthesized using a simple impregnation method at ambient temperature. Characterization of the catalyst was done through various techniques such as Fourier transform infrared (FTIR), energy dispersive X-ray, X-ray diffraction (XRD), transmission electron microscopy, scanning electron microscopy (SEM), elemental mapping, Raman spectroscopy, X-ray photoelectron spectroscopy, and thermogravimetric analysis (TGA) analyses. The kinetic study has shown the high catalytic performance of [DEIm][PF_6]@MOF-5 for the reduction of 4-nitrophenol (NP) compared to other catalysts. The catalyst also exhibited efficient electrochemical activity toward 4-NP reduction. The catalyst was recyclable for more than seven cycles without any significant loss in its catalytic performance. The recycled catalyst was further studied using XRD, FTIR, SEM, and TGA analyses to investigate the structural changes that occurred during the reaction. The catalyst maintained its structural integrity even after seven cycles.

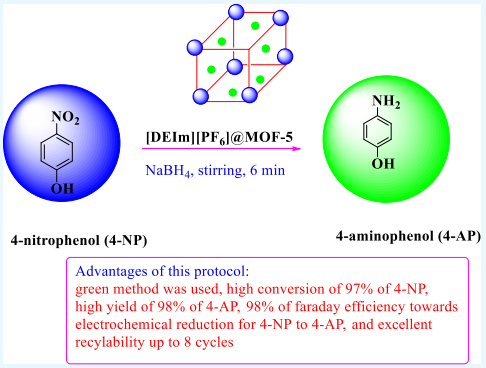

1. INTRODUCTION

Metal−organic frameworks (MOFs) have attracted significant attention from researchers in the last couple of decades due to their exclusive features, such as controllable pore sizes, high specific surface area, and unique surface chemistry.[1] As a result of these special features, various applications have been reported using MOFs, including catalysis,[2] gas storage and separation,[3] sensing,[4] luminescence,[5] drug delivery,[6] and 4-nitrophenol (4-NP) reduction.[7−10] MOF-5 is among the most widely used MOFs due to its remarkable properties, including an open skeleton structure, high porosity, high surface-to-volume ratio, and exceptional thermal stability. It is made up of a three-dimensional (3D) arrangement of organic linkers and a tetrahedrally coordinated Zn_4O metal cluster (e.g., terephthalic acid, 1,3,5-benzene tricarboxylic acid, etc.).[11] MOF-5's unrivaled characteristics make it an ideal material for various uses, such as in medicine,[12] Friedel−Crafts alkylation reactions,[13] hydrogen evolution reaction,[14] C−H activation and functionalization,[15] oxidation reactions,[16] Suzuki−Miyaura coupling reaction,[17] 4-NP reduction,[18−20] etc.

Because of a characteristic five-membered imidazole ring, imidazolium ionic liquids (ILs) have recently become superior functional materials. This is because of their nonflammability, low volatility, high thermal stability, and other characteristics.[21−25] They have been employed in organic reactions such as epoxide ring-opening reaction,[26] biodiesel synthesis,[27] to enhance oil recovery,[28] and 4-NP reduction.[29] Imidazolium ILs containing a hexafluorophosphate anion [PF_6^-] have gained attention because of their thermophysical properties, the solubility of gases on them, and some other applications.[30] However, ILs used in homogeneous catalysis have drawbacks, such as the need to use an enormous amount of ILs as catalysts or solvents, resulting in large quantities of waste that are difficult to get rid of. Therefore, such processes are not deemed environmentally benign. Thus, to overcome the drawbacks of homogeneous catalysis utilizing ILs and to make the catalyst heterogeneous, these ILs are impregnated on appropriate supports to integrate the benefits of ILs and the support materials such as silica,[31,32] chitosan,[33] cross-linked polymers,[34,35] magnetic nanoparticles (NPs),[36,37] carbon nanotubes,[38] MOFs,[39] etc.

Human health and safety issues have become important in the last few years as a result of serious environmental contamination. Among the various types of contaminants, nitroaromatic compounds (NACs) are not only very poisonous but also highly explosive.[40] Hence, the presence of NACs can lead to soil and water pollution, posing a significant

Received: September 7, 2022
Accepted: December 20, 2022
Published: January 19, 2023

Scheme 1. Synthesis of (a) MOF-5, (b) [DEIm][PF_6], and (c) Catalyst [DEIm][PF_6]@MOF-5

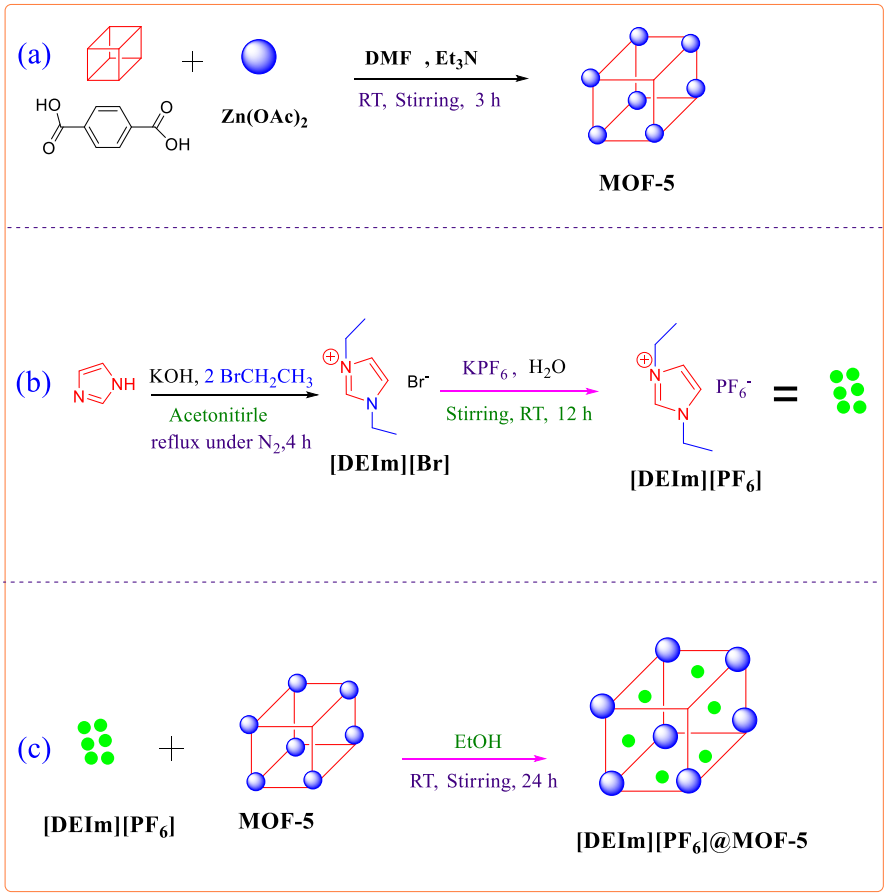

environmental hazard and cytotoxic effects in different biological systems.[41] Nitrophenols are identified as a significant toxic and carcinogenic pollutant in agricultural and industrial wastewater due to their water solubility.[42] They cause impedance to all living organisms in water resources.[43]

4-NP, a well-known organic hazard in industrial and agricultural wastewater, has precarious effects on the liver, kidneys, eyes, and the central nervous system. It has been classified as one of the most harmful and highly toxic pollutants by the US Environmental Protection Agency.[44−46] Because of the use of explosives, medications, insecticides, and dyes, it has become ubiquitous in the environment.[47] It is also reported that low quantities of 4-NP in water are hazardous to human health as well as aquatic life due to their mutagenesis effects and probable carcinogenicity.[48] In humans, the short-term inhalation of 4-NP has been proven to cause headaches, sleepiness, nausea, and cyanosis.[49] When damaging 4-NP is released into the soil, it can harm crops, water bodies, and the ecosystem.[50−54] Moreover, 4-NP is exceptionally stable and resistant to degradation naturally by microbes.[55−57] The removal of 4-NP from industrial wastewater is thus a complicated process. In comparison to the electrochemical[58] and photo-oxidation[59] strategies, catalytic reduction of 4-NP to 4-aminophenol (4-AP) is a more effective way to eliminate 4-NP. The amine functionality in 4-AP exists in various physiologically active natural compounds, dyes, and ligands for transition-metal catalyzed processes. Hence, reducing the nitro group into an amine group is an easy way to eliminate 4-NP from waste materials. 4-APs are also important intermediates in the synthesis of medicinal compounds, photographic materials, agrochemicals, polymers, and rubber materials because the amino group acts as a site for further derivatization.[60] As a result, the catalytic degradation of 4-NP to 4-AP using a heterogeneous catalyst is advantageous for environmental protection and has practical industrial applications.

Continuing our recent publications on the synthesis and applications of IL-based catalysts,[61−63] we present here the synthesis of [DEIm][PF_6]@MOF-5 as an effective and reusable catalyst for the reduction of 4-NP to 4-AP.

2. EXPERIMENTAL SECTION

2.1. Preparation of the Catalyst. *2.1.1. Preparation of MOF-5.* With minor modifications, MOF-5 was prepared according to a previously published technique.[64] Terephthalic acid (5.065 g, 30.5 mmol) and trimethylamine (8.5 mL) were dissolved in 400 mL dimethylformamide (DMF) in a usual manner to obtain a homogeneous solution. Zn $(OAc)_2 \cdot 2H_2O$ (16.99 g, 77.4 mmol) was dissolved in DMF (500 mL) and added to the homogeneous solution gradually for a period of 15 min with steady stirring. The mixture was further stirred for another 2.5 h. The as-obtained precipitate was filtered and steeped overnight in DMF (250 mL). It was then filtered off and submerged in $CHCl_3$ (350 mL, high-performance liquid chromatography grade). Over seven days, the solvent was exchanged three times: after two days, three days, and seven days. The product was evacuated overnight to a pressure of 10 mTorr after the bulk of the solvent was decanted. The product was activated for 6 h at 120 °C.

https://doi.org/10.1021/acsomega.2c05808
ACS Omega 2023, 8, 3785−3797

2.1.2. Preparation of IL [DEIm][PF$_6$]. 2.1.2.1. Preparation of IL (1,3 Diethyl Imidazolium Bromide) [DEIm][Br]. KOH (1.122 g, 20 mmol), 1-bromoethtane (2.1792 g, 20 mmol), and imidazole (0.6808 g, 10 mmol) were mixed in a round bottom flask containing acetonitrile (10 mL) and refluxed for about 4 h under a nitrogen atmosphere. Then it was cooled down to room temperature (RT), and the extra solvent was evaporated under vacuum to obtain [DEIm][Br].

2.1.2.2. Preparation of IL (Diethyl Imidazolium Bromide Hexafluorophosphate) [DEIm][PF$_6$]. The IL, diethyl imidazolium hexafluorophosphate ([DEIm][PF$_6$]) was prepared according to the literature with some modifications.[65−68] In a 50 mL round bottom flask, a mixture of diethyl imidazolium bromide (1.7599 g, 10 mmol), potassium hexafluorophosphate (22.0813 g, 11.79 mmol), and double distilled (DD) water (10 mL) was stirred at RT for 12 h. On completion of the reaction, the organic layer of the reaction mixture was washed with DD water (3 × 10 mL), and the product was dried under a vacuum for 8 h to obtain [DEIm][PF$_6$].

2.1.3. Preparation of the [DEIm][PF$_6$]@MOF-5. The catalyst, IL ([DEIm][PF$_6$]) supported on MOF-5 ([DEIm]-[PF$_6$]@MOF-5), was synthesized by a simple impregnation method. A mixture of [DEIm][PF$_6$] (1.080 g, 4 mmol) and MOF-5 (1 g) in ethanol (10 mL) was agitated at RT for 24 h. The resultant precipitate was filtered and rinsed three times with ethanol and oven-dried at 100 °C to obtain [DEIm][PF$_6$]@MOF-5 as a white powder.

2.2. Reduction of 4-NP. Reduction of 4-NP was achieved with the help of UV−visible spectroscopy screening between 200 and 550 nm. In the beginning, a standard solution of 4-NP in DD water (20 mg/L, 50 mL) was prepared for the catalytic reduction. In a 250 mL round bottom flask, a mixture of 25 mL of 4-NP solution (aqueous), 25 mL of freshly prepared sodium borohydride solution in DD water (100 mg/L), and 5 mg of [DEIm][PF$_6$]@MOF-5 was then added to it. The reaction mixture was kept under continuous stirring at RT. 1 mL of the reaction mixture was taken out every 30 s, diluted to 2.5 mL with DD, and promptly examined by a UV−visible spectrometer. The catalyst was filtered off, washed many times with DD water, and then oven-dried for further use.

3. RESULTS AND DISCUSSION

3.1. Synthesis and Characterization of the Catalyst. The synthesis of the catalyst [DEIm][PF$_6$]@MOF-5 is illustrated in Scheme 1

The Fourier transform infrared (FTIR) spectrum of MOF-5 is displayed in Figure 1a. Peaks appearing at 1600 and 1387 cm^{-1} were assigned to the symmetric and asymmetric stretching of C−O bonded to Zn.[69] Another peak at 1660 cm^{-1} was referred to the stretching vibration of the C═O group of terephthalic acid.[70] The peaks falling in the range 1135 to 952 cm^{-1} and 900 to 670 cm^{-1} corresponded to the in-plane and out-of-plane bending vibrations of the C−H bond of the benzene ring in the benzene-1,4-dicarboxylate linker, respectively.[71] The peak at 546 cm^{-1} was ascribed to Zn−O stretching. In the FTIR spectrum of [DEIm][Br] (Figure 1b), the peak at 3140 cm^{-1} was due to the C−H bond of imidazole ring,[63] whereas the peaks at 2974 and 2852 cm^{-1} were attributed to the −C−H stretching vibrations of −CH$_2$ and −CH$_3$ groups positioned at the nitrogen atoms of the imidazolium ring.[72] The peaks at 1631 and 1450 cm^{-1} were attributed to C═N and C−N stretching vibrations of the imidazole ring.[72] In the spectrum of ([DEIm][PF$_6$]) (Figure 1c), all the above characteristic peaks of diethyl imidazolium cation were present at their appropriate values. The presence of the [PF$_6$] anion was indicated by a sharp peak at 842 cm^{-1}

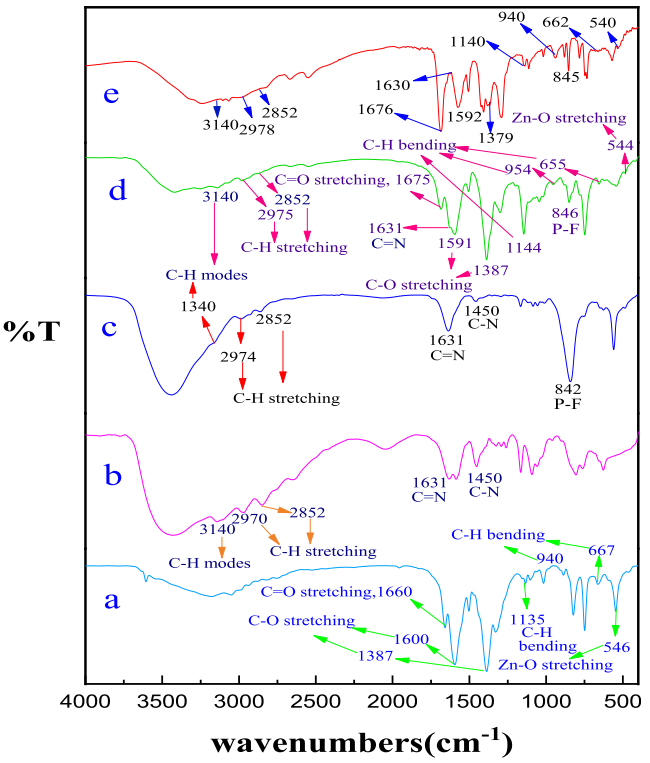

Figure 1. FTIR spectra of (a) MOF-5, (b) [DEIm][Br], (c) [DEIm][PF$_6$], (d) fresh catalyst [DEIm][PF$_6$]@MOF-5, and (e) recycled catalyst.

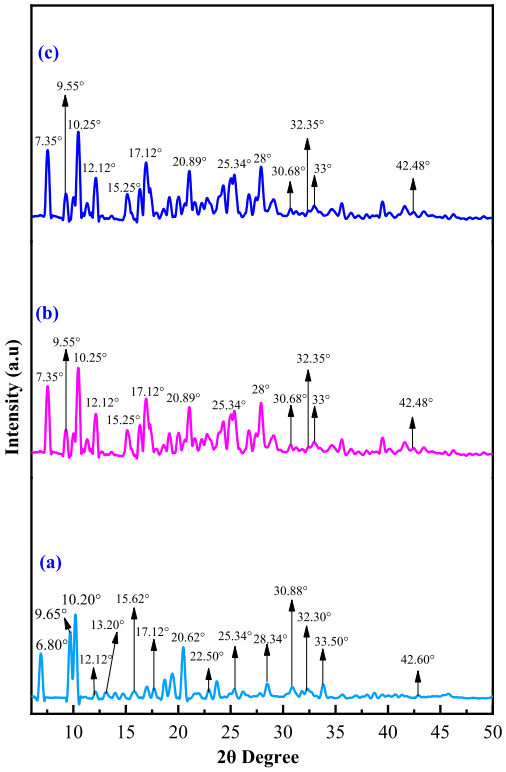

Figure 2. XRD spectra of (a) MOF-5, (b) fresh catalyst [DEIm][PF$_6$]@MOF-5, and (c) recycled catalyst.

https://doi.org/10.1021/acsomega.2c05808
ACS Omega 2023, 8, 3785−3797

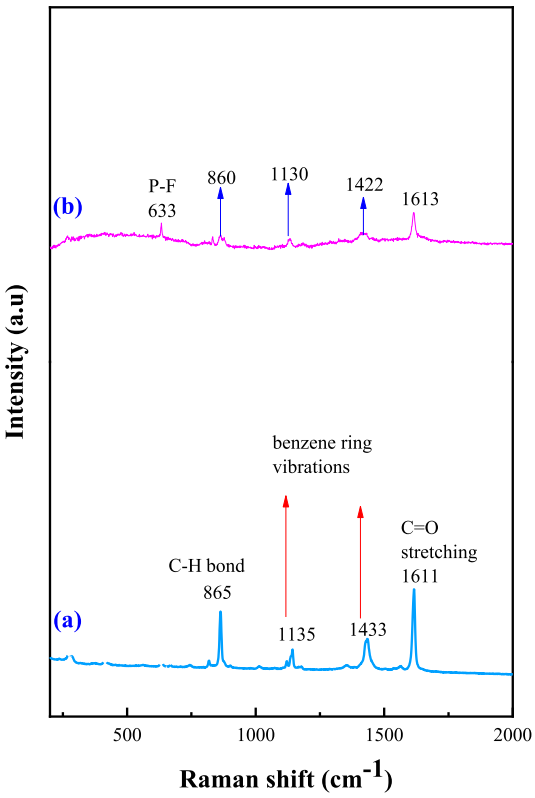

Figure 3. Raman spectra of (a) MOF-5 and (b) fresh catalyst [DEIm][PF_6]@MOF-5.

in the fingerprint region.[73] Furthermore, the presence of the [PF_6] anion was confirmed by the Raman spectrum of the catalyst (Figure 3b), showing a peak for the P−F bond at 633 cm^{-1}.

In the FTIR spectrum of catalyst [DEIm][PF_6]@MOF-5 (Figure 1d), all characteristic peaks of [DEIm][PF_6] and MOF-5 were present in the graph at their appropriate positions, confirming the formation of the catalyst [DEIm]-[PF_6]@MOF-5.

X-ray diffraction (XRD) studies of MOF-5, fresh catalyst [DEIm][PF_6]@MOF-5, and recycled catalyst are shown in Figure 2. Figure 2a shows the XRD pattern of MOF-5 displaying characteristic peaks at 2θ = 6.80, 9.65, 10.20, 12.12, 13.20, 15.62, 17.12, 20.62, 22.50, 25.34, 28.34, 30.88, 32.30, 33.50, and 42.60° which were consistent with that reported previously.[18,70,74] The XRD of the catalyst [DEIm][PF_6]@MOF-5 was almost similar to MOF-5, showing peaks almost at the same 2θ values (Figure 2b).

Raman spectroscopy of MOF-5 and catalyst [DEIm][PF_6]@MOF-5 was performed (Figure 3). In the Raman spectrum of MOF-5 (Figure 3a), a C═O stretching of the carboxylate group was observed at 1611 cm^{-1},[75] while in-plane bending vibrations of the benzene ring were obtained at 1433 and 1135 cm^{-1}. Another peak at 865 cm^{-1} was ascribed to out-of-plane distortion modes of the C−H bond. In the Raman spectrum of the catalyst [DEIm][PF_6]@MOF-5 (Figure 3b), all characteristic peaks of MOF-5 appeared with additional peaks at 1130 cm^{-1}, which might be due to different skeletal modes of vibrations of the imidazolium ring.[76] The band at 633 cm^{-1} (P−F system structure) confirmed the presence of the PF_6^- anion.[77]

We studied the surface morphology of MOF-5 and material [DEIm][PF_6]@MOF-5 using scanning electron microscopy (SEM) analysis (Figure 4). The SEM image of MOF-5 (Figure 4a,b) showed its characteristic cubic symmetry. The SEM image of the [DEIm][PF_6]@MOF-5 (Figure 4c) showed that the IL had been successfully doped on the surface of MOF-5 indicating that catalyst [DEIm][PF_6]@MOF-5 has been synthesized as visualized. Transmission electron microscopy (TEM) analysis also distinctly displayed the distribution of [DEIm][PF_6] on the surface of MOF-5 (Figure 5a,b). Further, energy dispersive X-ray (EDX) analysis showed the presence of C, N, O, F, P, and Zn elements in the material's structure

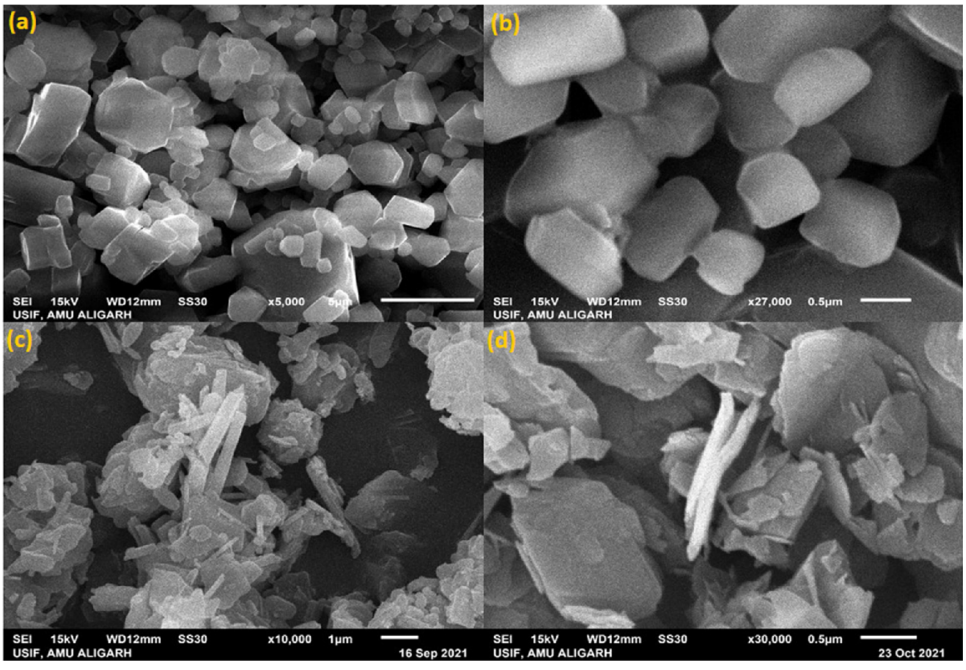

Figure 4. SEM images of (a, b) MOF-5, (c) fresh catalyst [DEIm][PF_6]@MOF-5, and (d) recycled catalyst.

https://doi.org/10.1021/acsomega.2c05808
ACS Omega 2023, 8, 3785−3797

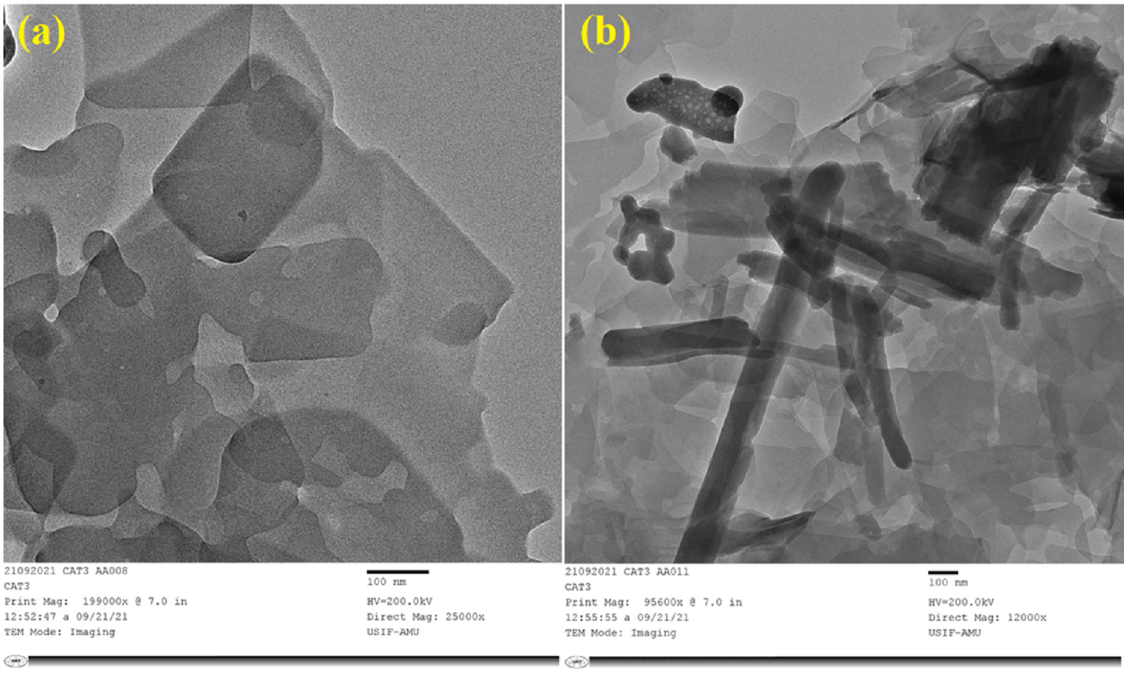

Figure 5. TEM images of (a) MOF-5 and (b) fresh catalyst [DEIm][PF_6]@MOF-5.

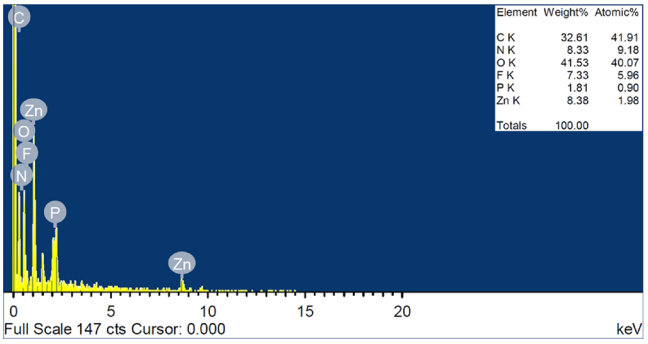

Figure 6. EDX analysis of catalyst [DEIm][PF_6]@MOF-5.

(Figure 6). The elemental mapping of individual elements C (Figure 7b), N (Figure 7c), O (Figure 7d), F (Figure 7e), P (Figure 7f), and Zn (Figure 7g) showed their uniform distribution throughout the material.

X-ray photoelectron spectroscopy (XPS) analysis was carried out to study the surface information and chemical composition of the catalyst [DEIm][PF_6]@MOF-5 (Figure 8). Figure 8a illustrates a scan survey of binding energies of the elements Zn 2p, F 1s, O 1s, N 1s, C 1s, and P 2p. In the XPS spectrum C 1s (Figure 8b), the peak at 284.88 eV was due to the C=C bond of MOF-5 and the imidazolium cation,[70,78] whereas the peak at 287.08 eV was ascribed to the C=O bond of MOF-5.[70] The binding energy at 401.2 V was attributed to N 1s of the C−N bond of the imidazolium cation (Figure 8c). Furthermore, the peaks at 685 and 133 eV (Figure 8d,e) corresponded to F 1s and P 2p of the [PF_6] anion, respectively.[79,80] The distinctive peak at 139 eV was ascribed to the P−F bond of the [PF_6] anion.[79] The XPS spectrum of Zn 2p (Figure 8f) showed two binding energy values at 1022.7 and 1045.5 eV, which were attributed to the $2p_{3/2}$ and $2p_{1/2}$ of Zn 2p in MOF-5.[81] The presence of Zn^{2+} species in MOF-5 was verified by a peak at 987.5 eV[81] in the survey XPS spectra (Figure 8a).

The thermal behavior of the catalyst [DEIm][PF_6]@MOF-5 was studied by TGA analysis, and dual weight loss was recorded (Figure 9). The first weight loss of 3.72% at 335 °C was attributed to the removal of water and DMF from the surface of MOF-5. In contrast, the second weight loss of 2.09% at 440 °C corresponded to the thermal decomposition of MOF-5.[82]

Potentiometric titration using an organic base (n-butylamine) was used to determine the acidity of solid acid catalysts. The computation of the electrode potential was determined by the acidic environment around the electrode membrane to calculate the acidity of the catalyst. The electrode potential (E_i) obtained from the titration was supposed to represent the total number of acid sites present in the titrated material. Figure 10 shows the potentiometric titration curves for MOF-5 and [DEIm][PF_6]@MOF-5 with E_i values of 138.29 and 148.29 mV, respectively. According to the literature, (E_i > 100 mV corresponded to a material having very strong acid sites, and −100 < E_i < 0 mV assigned to a material having weak acid sites),[83] which revealed that MOF-5 and [DEIm][PF_6]@MOF-5 had very strong acid sites. This was due to the acidic nature of MOF-5[84] and [DEIm][PF_6],[73] which boosted the E_i value of the final catalyst [DEIm][PF_6]@MOF-5.

3.2. Reduction of 4-NP. The catalytic performance of [DEIm][PF_6]@MOF-5 for the reduction of 4-NP to 4-AP was evaluated using a model reaction of 4-NP and $NaBH_4$ in the presence of [DEIm][PF_6]@MOF-5 in a quartz cuvette of 1 cm optical path length at RT.

First, $NaBH_4$ (100 mg/L, 4 mL) was added to the 4-NP solution (20 mg/L, 10 mL), and the solution was stirred for 2 min. The color of the mixture changed from light yellow to yellowish-green, and a high-intensity peak at 400 nm in the UV−vis absorption spectrum was observed due to the formation of 4-nitrophenolate anions. With the addition of [DEIm][PF_6]@MOF-5, the absorption peak at 400 nm remained unchanged, but the intensity of the peak slightly

https://doi.org/10.1021/acsomega.2c05808
ACS Omega 2023, 8, 3785−3797

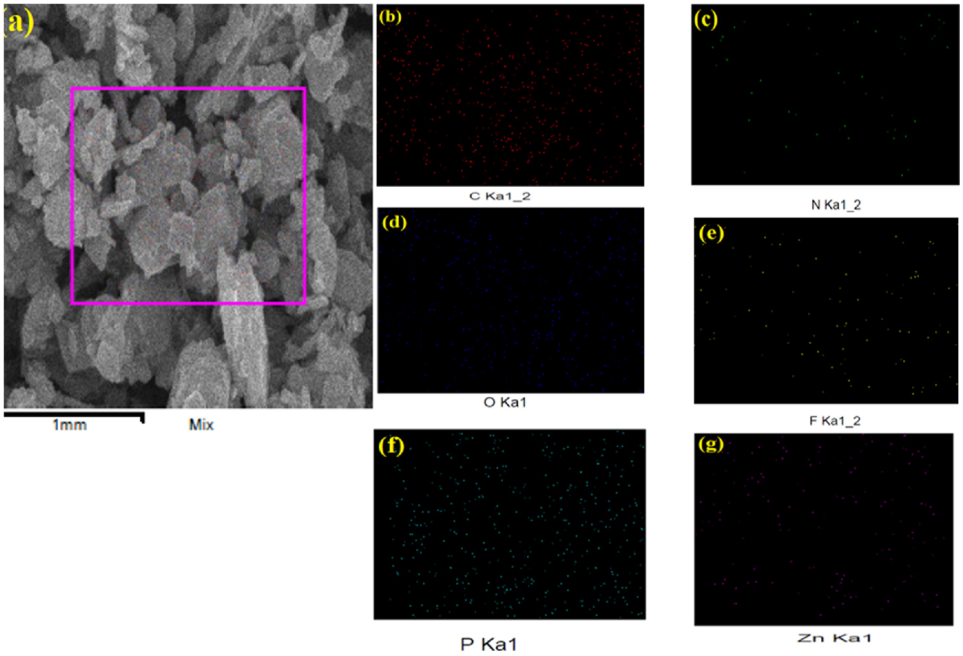

Figure 7. Elemental mapping analysis of (a) [DEIm][PF_6]@MOF-5 showing the presence of (b) carbon, (c) nitrogen, (d) oxygen, (e) fluorine, (f) phosphorous, and (g) zinc.

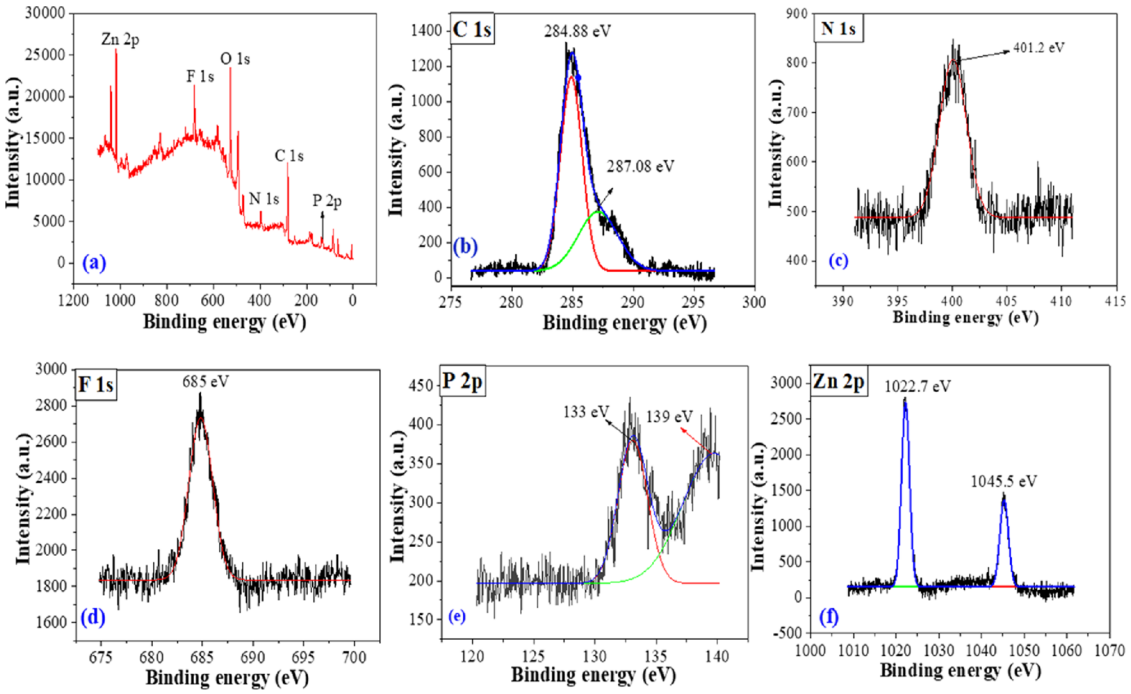

Figure 8. (a) Survey XPS spectrum of catalyst [DEIm][PF_6]@MOF-5, (b) high resolution XPS spectrum of C 1s, (c) high resolution XPS spectrum of N 1s, (d) high resolution XPS spectrum of F 1s, (e) high resolution XPS spectrum of P 2p, and (f) high resolution XPS spectrum of Zn 2p.

decreased (Figure 11). The intensity of the peak at 400 nm steadily reduced with a concurrent increase in the intensity of a new peak corresponding to 4-AP at 300 nm[85] at each time interval of 30 s. The formation of 4-AP was indicated by the piecemeal change in color of the solution from yellow to a brighter and brighter color.

Moreover, we have carried out the reduction of 4-NP to 4-AP using $NaBH_4$ as a reducing agent without using a catalyst, MOF-5, and IL [DEIm][PF_6] separately, and the results are summarized in Table 1. Without using any catalyst, the reaction could not proceed (Figure 12a). We obtained 49% of conversion of 4-NP to 4-AP by using [DEIm][PF_6] as a catalyst (Figure 12b). Then we used MOF-5 as a catalyst and obtained 94% of conversion of 4-NP to 4-AP (Figure 12c).

The turnover number (TON) measures a material's catalytic performance for a specific reaction. It is the number of moles of product isolated per catalyst active site. The turnover frequency (TOF) is the TON per hour of reaction time,

https://doi.org/10.1021/acsomega.2c05808
ACS Omega 2023, 8, 3785−3797

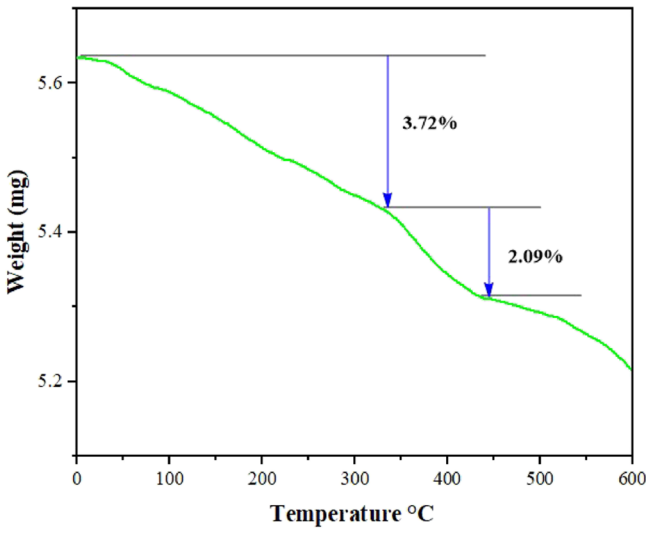

Figure 9. TGA analysis of catalyst [DEIm][PF_6]@MOF-5.

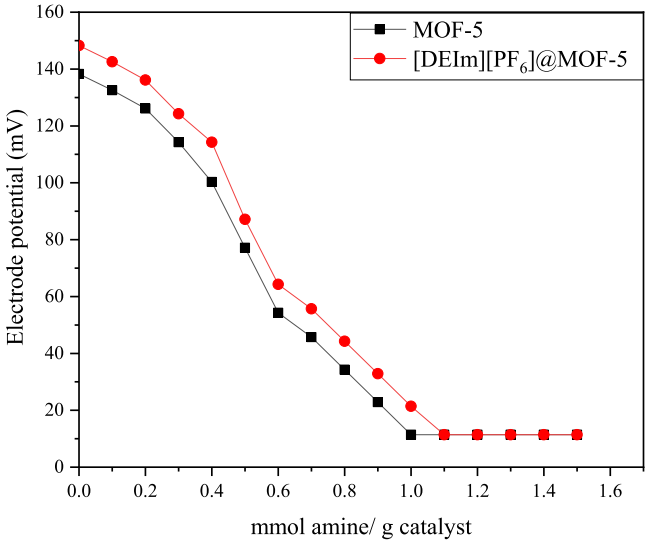

Figure 10. Potentiometric titration curve of MOF-5 and [DEIm]-[PF_6]@MOF-5.

Table 1. Catalytic Activities of Different Catalysts for 4-NP Reduction[a]

no.	catalyst	conversion %	4-AP yield
1	No catalyst		
2	[DEIm][PF_6]	49	50
3	MOF-5	94	95
4	[DEIm][PF_6]@MOF-5	97	98

[a]Reaction conditions: 4-NP (20 mg/L, 10 mL); $NaBH_4$ (100 mg/L, 4 mL); catalyst (5 mg); time = 6 min.

indicating the catalyst's efficiency. The TON (1.44) and TOF (14.38) calculations revealed that the catalyst was effective for the reduction of 4-NP to 4-AP. The catalytic activity of [DEIm][PF_6]@MOF-5 was compared with previous catalysts, as shown in Table 2.

3.3. Mechanism of Reduction. As confirmed from the previous studies, the reduction of 4-NP does not occur only with sodium borohydride ($NaBH_4$, as a hydrogen generator) because of the high kinetic barrier between mutually repelling negative ions BH_4^- and 4-NP.[85] Hence, a medium was required to minimize the kinetic barrier. A study revealed that electron transfer from $NaBH_4$ to 4-NP could be possible using gold NPs as a medium. The reaction was supposed to occur in two steps: diffusion adsorption of 4-NP on NP surfaces and electron transfer.[89] Other researchers also supported this mechanism using silver[90] and copper NPs by overcoming the reaction's kinetic barrier. It was concluded that anything that enhances electron transport could boost the reduction process.[91]

In the present work, we have synthesized [DEIm][PF_6]@MOF-5 as a heterogeneous catalyst to promote the reduction of 4-NP to 4-AP. The reaction was observed to progress efficiently in the presence of a minute quantity of [DEIm]-[PF_6]@MOF-5, where [DEIm][PF_6] helps in the adsorption of 4-NP and $NaBH_4$ on the surface of the catalyst (MOF-5) thereby lowering the kinetic barrier. Then, the transfer of the electron from BH_4^- (donor) to the nitro groups of 4-NP (acceptor) was mediated by the catalyst surface (MOF-5). The final product (4-AP) was formed in three steps.[92] In the first step, 4-NP was reduced to 4-nitrosophenol with the removal of

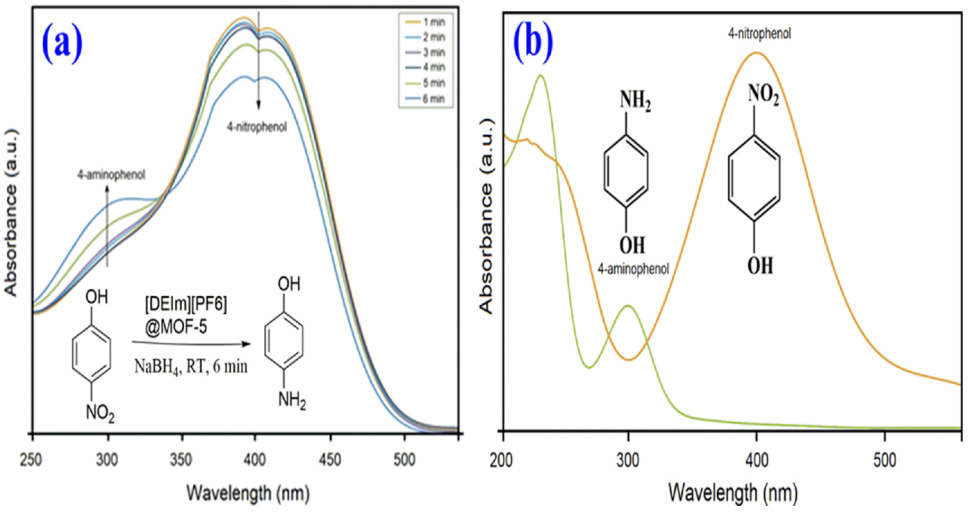

Figure 11. (a) Reduction of 4-NP to 4-AP using [DEIm][PF_6]@MOF-5 at different time intervals and (b) complete reduction of 4-NP to 4-AP using [DEIm][PF_6]@MOF-5 after 30 min.

https://doi.org/10.1021/acsomega.2c05808
ACS Omega 2023, 8, 3785−3797

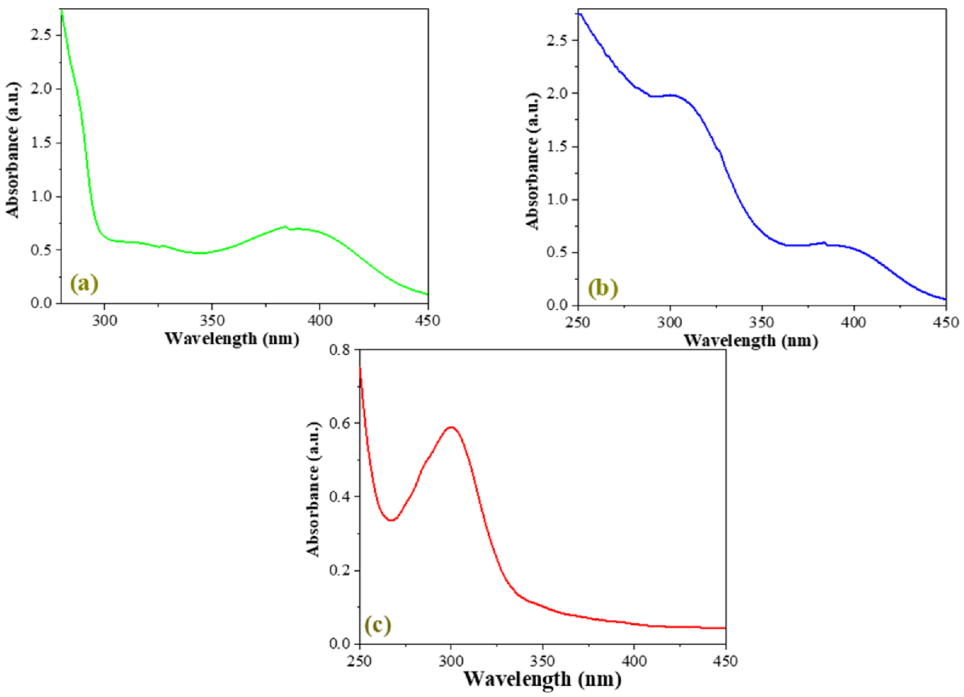

Figure 12. Reduction of 4-NP to 4-AP using $NaBH_4$ as a reducing agent in the presence of (a) no catalyst, (b) [DEIm][PF_6], and (c) MOF-5.

Table 2. Comparison of Catalytic Activity of [DEIm][PF_6]@MOF-5 for the Reduction of 4-NP

no.	catalyst	TOF (h^{-1})	reference
1	Au@[C_4C_{16}Im]Br	3×10^{-3}	86
2	$HAuCl_4$·3H2O	6.6	87
3	Au/graphene hydrogel	11.4	88
4	**[DEIm][PF_6]@MOF-5**	**14.38**	**this work**

Scheme 2. Plausible Mechanism for the Reduction of 4-NP to 4-AP

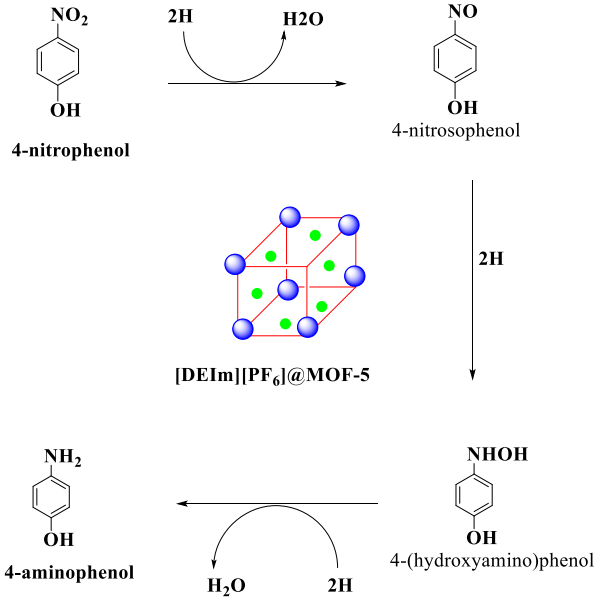

water followed by the second step in which 4-nitrosophenol was further reduced to 4-(hydroxyamino) phenol which ultimately gave 4-AP in the final step with the subsequent elimination of water molecule. In Scheme 2, a plausible mechanism is shown.

3.4. Kinetic Study. C_t/C_0 was used to compute the reaction conversion and assessed in terms of the relative intensity of UV−vis absorbance (A_t/A_0) at 400 nm. C_t is the concentration of 4-NP at response time t, and C_0 denotes the starting concentration. Figure 13a shows the C_t/C_0 versus response time (min) plot. The linear relationship between $\ln(C_t/C_0)$ and reaction time, as shown in Figure 13b, revealed that the reaction is of first-order for the reduction of 4-NP. The following kinetic equation may be used to obtain the first-order rate constant:

$$\ln(C_t/C_0) = \ln(A_t/A_0) = -Kt$$

where, A_t is the absorbance at any time t (min); A_0 is the absorbance at time $t = 0$, and K is the apparent rate constant, estimated from the slope of $\ln(C_t/C_0)$ versus t. K of [DEIm][PF_6] @MOF-5 was calculated as 0.945 min^{-1}. Also, the activity factor (defined as the ratio of rate constant over the total mass of catalyst) of [DEIm][PF_6]@MOF-5 was calculated to be 63 min^{-1} mg^{-1}. The catalytic performance of [DEIm][PF_6]@MOF-5 was compared with reported catalysts under similar reaction conditions. For comparison, the rate constant of Au@[C_4C_{16}Im]Br and Zn MOF@C was reported as 0.0066 min^{-1}, 0.2856 min^{-1}, respectively,[86,93] and the rate constant and activity factor of KCC-1−IL/Au were reported as 0.718 min^{-1}, 57.4 min^{-1} mg^{-1}, respectively.[29] The data showed that [DEIm][PF_6]@MOF-5 had higher catalytic activity and activity factor than the other reported catalysts.

3.5. Electrochemical Studies of [DEIm][PF_6]@MOF-5 toward 4-Nitro Phenol Reduction. We also investigated the reduction of 4-NP using cyclic voltammetry (CV) analysis on a bare glassy carbon electrode (GCE) surface. Figure 14a shows the cyclic voltammogram obtained at [DEIm][PF_6]@MOF-5/GCE in 0.2 M phosphate buffer solutions (PBS) (pH 6) containing 1 mM 4-NP where the potential was scanned from −0.8 to +1.2 V at a scan rate of 0.1 V/s. It was shown that the

https://doi.org/10.1021/acsomega.2c05808
ACS Omega 2023, 8, 3785−3797

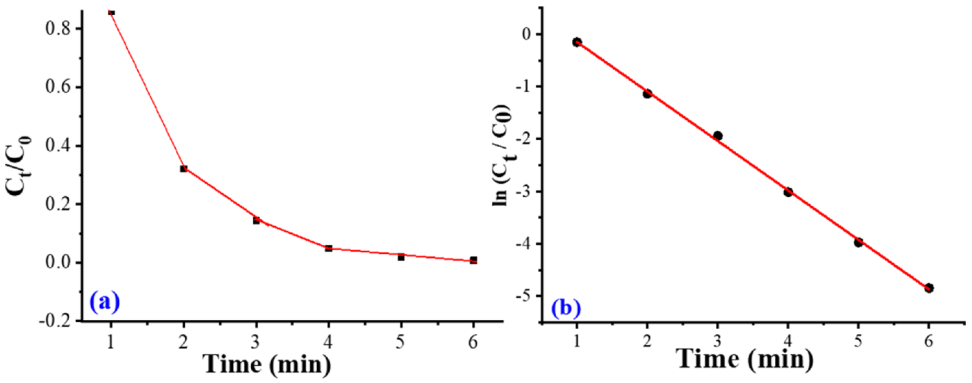

Figure 13. Plots of (a) C_t/C_0 and (b) $\ln(C_t/C_0)$ versus reaction time for the reduction of 4-NP over [DEIm][PF_6]@MOF-5.

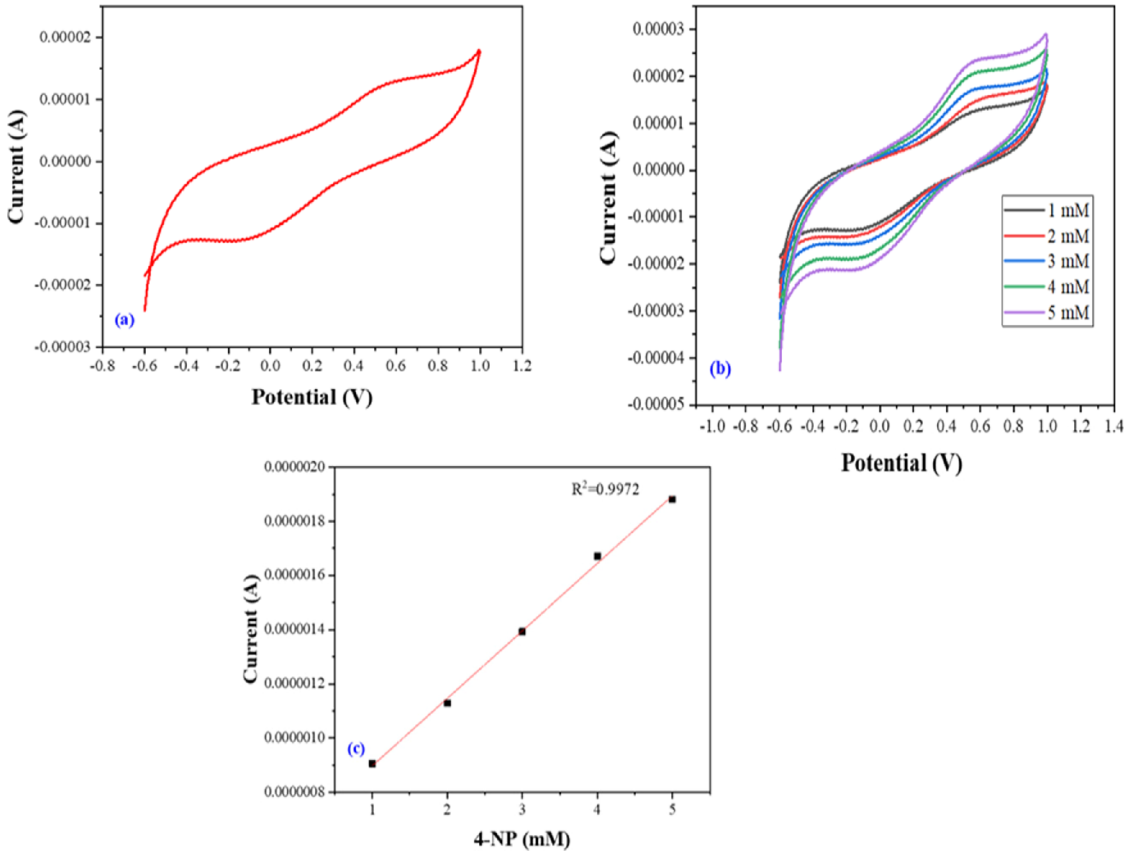

Figure 14. (a) Cyclic voltammogram of [DEIm][PF_6]@MOF-5 in PBS (pH 6) at scan rate 0.1 V/s in the presence of 1 mM 4-NP on GCE, (b) cyclic voltammograms of [DEIm][PF_6]@MOF-5 in PBS (pH 6) at scan rate 0.1 V/s in the presence of different concentrations of 4-NP, and (c) calibration plot of the 4-NP sensor.

reduction of 4-NP took place at −0.18 V with an enhanced peak current of 12.8 μA.

Figure 14b displays the cyclic voltammograms for various concentrations of 4-NP at [DEIm][PF_6]@MOF-5/GCE in 0.2 M PBS (pH 6) at a scan rate of 0.1 V/s. The reduction peak current increases linearly with increasing concentration (1, 2, 3, 4, and 5 mM) (Figure 14c), resulting in [DEIm][PF_6]@MOF-5 having efficient electrochemical activity toward the reduction of 4-NP.

Figure 15 displays parameters of conversion of 4-NP, 4-AP yield, and Faraday efficiency (FE) during eight successive cycles to assess the electrochemical reduction of 4-NP to 4-AP over [DEIm][PF_6]@MOF-5. The FE can be calculated as follows:[94,95]

$$\mathrm{FE} = 3 \times F \times [4 - \mathrm{AP}] \times V17 \times Q$$

where F is the Faraday constant, [4-AP] is the concentration of resultant 4-AP, V is the volume of the cathodic reaction electrolyte, and Q is the quantity of applied charge. The results of the parameters were 98% of conversion of 4-NP, 98% of yield of 4-AP, and 98% of FE during eight successive cycles of conversion of 4-NP to 4-AP over [DEIm][PF_6]@MOF-5. Thus, it was revealed that [DEIm][PF_6]@MOF-5 had high stability and efficiency toward the electrochemical reduction of 4-NP to 4-AP.

3.6. Recyclability of the Catalyst. To demonstrate the catalyst effectiveness of the catalyst, we executed a recyclability experiment using [DEIm][PF_6]@MOF-5 throughout consec-

https://doi.org/10.1021/acsomega.2c05808
ACS Omega 2023, 8, 3785−3797

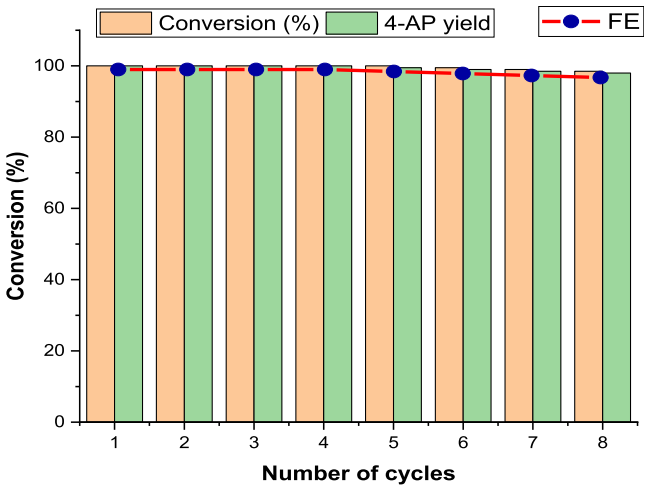

Figure 15. Conversion of 4-NP, 4-AP yield, and FE during eight successive cycles of conversion of 4-NP to 4-AP over [DEIm][PF_6]@MOF-5.

utive cycles of 4-NP reduction. Using the same method of the reduction reaction, it was found that [DEIm][PF_6]@MOF-5 retained the catalytic activity for more than seven cycles affording 4-AP in excellent yield with insignificant loss in catalytic performance (Figure 16). The recovered catalyst was studied by XRD, FTIR, and SEM analyses. The FTIR spectrum of the recycled catalyst (Figure 1d) showed that all distinctive peaks (1676, 1630, 845, and 540 cm^{-1}) of the recycled catalyst (8th cycle) were present when compared to the fresh catalyst (Figure 1c). The XRD spectrum of the recovered catalyst (Figure 2c) showed no remarkable structural change in the material after the seventh cycle (Figure 2b). The surface morphology of the recycled catalyst was also unchanged (Figure 4d).

4. CONCLUSIONS

In conclusion, we have designed and synthesized a novel, proper, highly efficient, and ecofriendly IL-supported MOF-5, [DEIm][PF_6]@MOF-5, as a heterogeneous catalyst. The as-prepared catalyst showed excellent catalytic activity for the reduction of 4-NP to 4-AP in the presence of $NaBH_4$ in just 6 min at RT with excellent yield (98%). Moreover, after consecutive eight cycles of the reduction reaction, [DEIm]-[PF_6]@MOF-5 still maintained high conversion efficiencies of over (97%). The notable features of our ecofriendly method include high product yield (98%), reusability of up to eight cycles, and high thermal stability of the material.

■ ASSOCIATED CONTENT

Supporting Information

The Supporting Information is available free of charge at https://pubs.acs.org/doi/10.1021/acsomega.2c05808.

Materials and reagents, details of instruments used for the analyses like FTIR, XRD, Raman, TGA, XPS, SEM, TEM, EDX, CV, and UV−vis instruments (PDF)

■ AUTHOR INFORMATION

Corresponding Author

Zeba N. Siddiqui − *Green Chemistry Laboratory, Organic Chemistry Division, Department of Chemistry, Aligarh Muslim University, Aligarh, Uttar Pradesh 202002, India;* orcid.org/0000-0002-0952-8608; Email: zeba.ch@amu.ac.in, siddiqui_zeba@yahoo.co.in

Author

Abdulaziz Abdullah Qasem Ali − *Green Chemistry Laboratory, Organic Chemistry Division, Department of Chemistry, Aligarh Muslim University, Aligarh, Uttar Pradesh 202002, India*

Complete contact information is available at: https://pubs.acs.org/10.1021/acsomega.2c05808

Notes

The authors declare no competing financial interest.

■ ACKNOWLEDGMENTS

The authors are thankful to University Sophisticated Instrumentation Facility (USIF), AMU, Aligarh for EDX, SEM, TEM, and Elemental Mapping facilities, and IIT Roorkee, Roorkee for XPS analysis.

■ REFERENCES

(1) Maina, J. W.; Pozo-Gonzalo, C.; Kong, L.; Schütz, J.; Hill, M.; Dumée, L. F. Metal Organic Framework Based Catalysts for CO2 Conversion. *Mater. Horiz.* **2017**, *4*, 345−361.

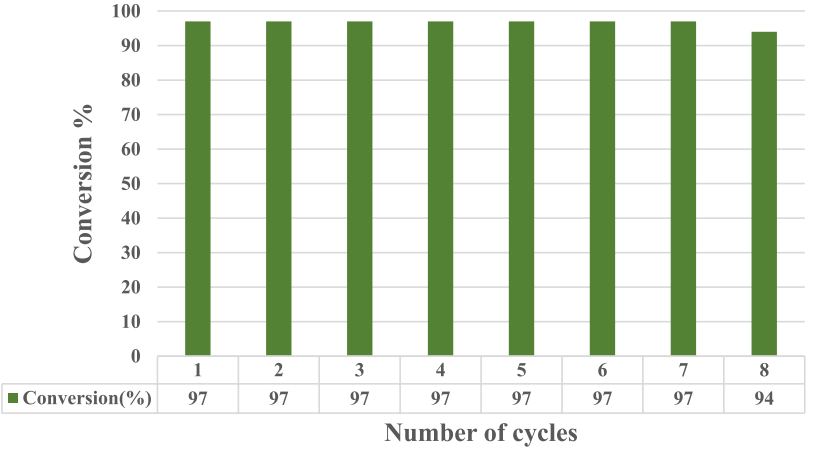

Figure 16. Recycling study of [DEIm][PF_6]@MOF-5 for the reduction of 4-NP to 4-AP.

https://doi.org/10.1021/acsomega.2c05808
ACS Omega 2023, 8, 3785−3797

(2) Liu, J.; Chen, L.; Cui, H.; Zhang, J.; Zhang, L.; Su, C. Y. Applications of Metal-Organic Frameworks in Heterogeneous Supramolecular Catalysis. *Chem. Soc. Rev.* **2014**, *43*, 6011−6061.
(3) Nandasiri, M. I.; Jambovane, S. R.; McGrail, B. P.; Schaef, H. T.; Nune, S. K. Adsorption, Separation, and Catalytic Properties of Densified Metal-Organic Frameworks. *Coord. Chem. Rev.* **2016**, *311*, 38−52.
(4) Lin, R. B.; Liu, S. Y.; Ye, J. W.; Li, X. Y.; Zhang, J. P. Photoluminescent Metal−Organic Frameworks for Gas Sensing. *Adv. Sci.* **2016**, *3*, No. 1500434.
(5) Rocha, J.; Brites, C. D. S.; Carlos, L. D. Lanthanide Organic Framework Luminescent Thermometers. *Chem. - Eur. J.* **2016**, *22*, 14782−14795.
(6) Giménez-Marqués, M.; Hidalgo, T.; Serre, C.; Horcajada, P. Nanostructured Metal-Organic Frameworks and Their Bio-Related Applications. *Coord. Chem. Rev.* **2016**, *307*, 342−360.
(7) Jin, L.; Zhao, X.; Ye, J.; Qian, X.; Dong, M. MOF-Derived Magnetic Ni-Carbon Submicrorods for the Catalytic Reduction of 4-Nitrophenol. *Catal. Commun.* **2018**, *107*, 43−47.
(8) Duan, C.; Liu, C.; Meng, X.; Lu, W.; Ni, Y. Fabrication of Carboxymethylated Cellulose Fibers Supporting Ag NPs@MOF-199s Nanocatalysts for Catalytic Reduction of 4-Nitrophenol. *Appl. Organomet. Chem.* **2019**, *33*, No. e4865.
(9) Khan, A.; Wei, D.; Wang, Z.; Su, X.; Wang, J.; Alam, S.; Wang, L.; Wu, R.; Maloletnev, A. S.; Yang, C. MOF-Derived Nickel−cobalt Bimetal Oxide Nanostructures as a Cooperative Catalyst for the Reduction of 4-Nitrophenol. *J. Chem. Technol. Biotechnol.* **2021**, *96*, 697−703.
(10) Ahsan, M. A.; Deemer, E.; Fernandez-Delgado, O.; Wang, H.; Curry, M. L.; El-Gendy, A. A.; Noveron, J. C. Fe Nanoparticles Encapsulated in MOF-Derived Carbon for the Reduction of 4-Nitrophenol and Methyl Orange in Water. *Catal. Commun.* **2019**, *130*, No. 105753.
(11) Li, J.; Cheng, S.; Zhao, Q.; Long, P.; Dong, J. Synthesis and Hydrogen-Storage Behavior of Metal-Organic Framework MOF-5. *Int. J. Hydrogen Energy* **2009**, *34*, 1377−1382.
(12) Luo, Z.; Fan, S.; Gu, C.; Liu, W.; Chen, J.; Li, B.; Liu, J. Metal−Organic Framework (MOF)-Based Nanomaterials for Biomedical Applications. *Curr. Med. Chem.* **2019**, *26*, 3341−3369.
(13) Phan, N. T. S.; Le, K. K. A.; Phan, T. D. MOF-5 as an Efficient Heterogeneous Catalyst for Friedel-Crafts Alkylation Reactions. *Appl. Catal. A Gen.* **2010**, *382*, 246−253.
(14) Yang, H. M.; Song, X. L.; Yang, T. L.; Liang, Z. H.; Fan, C. M.; Hao, X. G. Electrochemical Synthesis of Flower Shaped Morphology MOFs in an Ionic Liquid System and Their Electrocatalytic Application to the Hydrogen Evolution Reaction. *RSC Adv.* **2014**, *4*, 15720−15726.
(15) Park, T.; Hickman, A. J.; Koh, K.; Martin, S.; Wong-foy, A. G.; Sanford, M. S.; Matzger, A. J. Highly Dispersed Palladium (II) in a Defective Metal-Organic. *J. Am. Chem. Soc.* **2011**, 20138−20141.
(16) Li, J.; Chen, Y.; Tang, Y.; Li, S.; Dong, H.; Li, K.; Han, M.; Lan, Y. Q.; Bao, J.; Dai, Z. Metal-Organic Framework Templated Nitrogen and Sulfur Co-Doped Porous Carbons as Highly Efficient Metal-Free Electrocatalysts for Oxygen Reduction Reactions. *J. Mater. Chem. A* **2014**, *2*, 6316−6319.
(17) Dong, W.; Zhang, L.; Wang, C.; Feng, C.; Shang, N.; Gao, S.; Wang, C. Palladium Nanoparticles Embedded in Metal-Organic Framework Derived Porous Carbon: Synthesis and Application for Efficient Suzuki-Miyaura Coupling Reactions. *RSC Adv.* **2016**, *6*, 37118−37123.
(18) Samuel, M. S.; Bhattacharya, J.; Parthiban, C.; Viswanathan, G.; Pradeep Singh, N. D. Ultrasound-Assisted Synthesis of Metal Organic Framework for the Photocatalytic Reduction of 4-Nitrophenol under Direct Sunlight. *Ultrason. Sonochem.* **2018**, *49*, 215−221.
(19) Huang, G.; Yang, L.; Ma, X.; Jiang, J.; Yu, S. H.; Jiang, H. L. Metal-Organic Framework-Templated Porous Carbon for Highly Efficient Catalysis: The Critical Role of Pyrrolic Nitrogen Species. *Chem. - Eur. J.* **2016**, *22*, 3470−3477.
(20) Panda, J.; Biswal, S. P.; Jena, H. S.; Mitra, A.; Samantray, R.; Sahu, R. Role of Lewis Acid Metal Centers in Metal−Organic Frameworks for Ultrafast Reduction of 4-Nitrophenol. *Catalysts* **2022**, *12*, 494.
(21) Binnemans, K. Lanthanides and Actinides in Ionic Liquids. *Compr. Inorg. Chem. II* **2013**, *2*, 641−673.
(22) Petkovic, M.; Seddon, K. R.; Rebelo, L. P. N.; Pereira, C. S. Ionic Liquids: A Pathway to Environmental Acceptability. *Chem. Soc. Rev.* **2011**, *40*, 1383−1403.
(23) Jutz, F.; Andanson, J.-M.; Baiker, A. Ionic Liquids and Dense Carbon Dioxide: A Beneficial Biphasic System for Catalysis. *Chem.Rev.* **2011**, *111*, 322−353.
(24) Dupont, J.; De Souza, R. F.; Suarez, P. A. Z. Ionic Liquid (Molten Salt) Phase Organometallic Catalysis. *Chem. Rev.* **2002**, *102*, 3667−3692.
(25) Zakrzewska, M. E.; Bogel-Łukasik, E.; Bogel-Łukasik, R. Ionic Liquid-Mediated Formation of 5-Hydroxymethylfurfural— A Promising Biomass-Derived Building Block. *Chem. Rev.* **2011**, *111*, 397−417.
(26) Rad, M. N. S.; Behrouz, S. The Base-Free Chemoselective Ring Opening of Epoxides with Carboxylic Acids Using [Bmim]Br: A Rapid Entry into 1,2-Diol Mono-Esters Synthesis. *Mol. Divers.* **2013**, *17*, 9−18.
(27) Fan, P.; Xing, S.; Wang, J.; Fu, J.; Yang, L.; Yang, G.; Miao, C.; Lv, P. Sulfonated Imidazolium Ionic Liquid-Catalyzed Transesterification for Biodiesel Synthesis. *Fuel* **2017**, *188*, 483−488.
(28) Nandwani, S. K.; Malek, N. I.; Lad, V. N.; Chakraborty, M.; Gupta, S. Study on Interfacial Properties of Imidazolium Ionic Liquids as Surfactant and Their Application in Enhanced Oil Recovery. *Colloids Surf. A Physicochem. Eng. Asp.* **2017**, *516*, 383−393.
(29) Yang, H.; Li, S.; Zhang, X.; Wang, X.; Ma, J. Imidazolium Ionic Liquid-Modified Fibrous Silica Microspheres Loaded with Gold Nanoparticles and Their Enhanced Catalytic Activity and Reusability for the Reduction of 4-Nitrophenol. *J. Mater. Chem. A* **2014**, *2*, 12060−12067.
(30) Llovell, F.; Vilaseca, O.; Vega, L. F. Thermodynamic Modeling of Imidazolium-Based Ionic Liquids with the [PF 6] - Anion for Separation Purposes. *Sep. Sci. Technol.* **2012**, *47*, 399−410.
(31) Dharman, M. M.; Choi, H. J.; Kim, D. W.; Park, D. W. Synthesis of Cyclic Carbonate through Microwave Irradiation Using Silica-Supported Ionic Liquids: Effect of Variation in the Silica Support. *Catal. Today* **2011**, *164*, 544−547.
(32) Han, L.; Choi, H. J.; Choi, S. J.; Liu, B.; Park, D. W. Ionic Liquids Containing Carboxyl Acid Moieties Grafted onto Silica: Synthesis and Application as Heterogeneous Catalysts for Cycloaddition Reactions of Epoxide and Carbon Dioxide. *Green Chem.* **2011**, *13*, 1023−1028.
(33) Sun, J.; Wang, J.; Cheng, W.; Zhang, J.; Li, X.; Zhang, S.; She, Y. Chitosan Functionalized Ionic Liquid as a Recyclable Biopolymer-Supported Catalyst for Cycloaddition of CO2. *Green Chem.* **2012**, *14*, 654−660.
(34) Xie, Y.; Zhang, Z.; Jiang, T.; He, J.; Han, B.; Wu, T.; Ding, K. CO2 Cycloaddition Reactions Catalyzed by an Ionic Liquid Grafted onto a Highly Cross-Linked Polymer Matrix. *Angew. Chem., Int. Ed.* **2007**, *46*, 7255−7258.
(35) Sun, J.; Cheng, W.; Fan, W.; Wang, Y.; Meng, Z.; Zhang, S. Reusable and Efficient Polymer-Supported Task-Specific Ionic Liquid Catalyst for Cycloaddition of Epoxide with CO2. *Catal. Today* **2009**, *148*, 361−367.
(36) Zheng, X.; Luo, S.; Zhang, L.; Cheng, J. P. Magnetic Nanoparticle Supported Ionic Liquid Catalysts for CO2 Cycloaddition Reactions. *Green Chem.* **2009**, *11*, 455−445.
(37) Li, P. H.; Li, L. B.; Hu, H. C.; Zhao, X. N.; Zhang, Z. H. Ionic Liquid Supported on Magnetic Nanoparticles as Highly Efficient and Recyclable Catalyst for the Synthesis of β-Keto Enol Ethers. *Catal. Commun.* **2014**, *46*, 118−122.
(38) Han, L.; Li, H.; Choi, S. J.; Park, M. S.; Lee, S. M.; Kim, Y. J.; Park, D. W. Ionic Liquids Grafted on Carbon Nanotubes as Highly Efficient Heterogeneous Catalysts for the Synthesis of Cyclic Carbonates. *Appl. Catal. A Gen.* **2012**, *429-430*, 67−72.

https://doi.org/10.1021/acsomega.2c05808
ACS Omega 2023, 8, 3785−3797

(39) Kim, J.; Kim, S. N.; Jang, H. G.; Seo, G.; Ahn, W. S. CO2 Cycloaddition of Styrene Oxide over MOF Catalysts. *Appl. Catal. A Gen.* **2013**, *453*, 175−180.
(40) Wu, X. X.; Fu, H. R.; Le Han, M.; Zhou, Z.; Ma, L. F. Tetraphenylethylene Immobilized Metal-Organic Frameworks: Highly Sensitive Fluorescent Sensor for the Detection of Cr2O72- and Nitroaromatic Explosives. *Cryst. Growth Des.* **2017**, *17*, 6041−6048.
(41) Purohit, V.; Basu, A. K. Mutagenicity of Nitroaromatic Compounds. *Chem. Res. Toxicol.* **2000**, *13*, 673−692.
(42) Ali, I.; Asim, M.; Khan, T. A. Low Cost Adsorbents for the Removal of Organic Pollutants from Wastewater. *J. Environ. Manage.* **2012**, *113*, 170−183.
(43) Dhanavel, S.; Manivannan, N.; Mathivanan, N.; Gupta, V. K.; Narayanan, V.; Stephen, A. Preparation and Characterization of Cross-Linked Chitosan/Palladium Nanocomposites for Catalytic and Antibacterial Activity. *J. Mol. Liq.* **2018**, *2018*, 32−41.
(44) Zhang, C.; Zhang, R.; He, S.; Li, L.; Wang, X.; Liu, M.; Chen, W.; Zhang, C.; Zhang, R.; He, S.; Li, L.; Wang, X.; Liu, M. 4-Nitrophenol Reduction by Encaging Single PtPd Nanocube in Nitrogen-Doped Hollow Carbon Nanosphere. *ChemCatChem* **2016**, *9*, 980−986.
(45) Zhu, X. Y.; Lv, Z. S.; Feng, J. J.; Yuan, P. X.; Zhang, L.; Chen, J. R.; Wang, A. J. Controlled Fabrication of Well-Dispersed AgPd Nanoclusters Supported on Reduced Graphene Oxide with Highly Enhanced Catalytic Properties towards 4-Nitrophenol Reduction. *J. Colloid Interface Sci.* **2018**, *516*, 355−363.
(46) Du, C.; He, S.; Gao, X.; Chen, W. Hierarchical Cu@MnO2 Core−Shell Nanowires: A Nonprecious-Metal Catalyst with an Excellent Catalytic Activity Toward the Reduction of 4-Nitrophenol. *ChemCatChem* **2016**, *8*, 2885−2889.
(47) Wang, Y.; Xie, Y.; Sun, H.; Xiao, J.; Cao, H.; Wang, S. Hierarchical Shape-Controlled Mixed-Valence Calcium Manganites for Catalytic Ozonation of Aqueous Phenolic Compounds. *Catal. Sci. Technol.* **2016**, *6*, 2918−2929.
(48) Baghbamidi, S. E.; Hassankhani, A.; Sanchooli, E.; Sadeghzadeh, S. M. The Reduction of 4-Nitrophenol and 2-Nitroaniline by Palladium Catalyst Based on a KCC-1/IL in Aqueous Solution. *Appl. Organomet. Chem.* **2018**, *32*, 1−8.
(49) Ansar, S. M.; Kitchens, C. L. Impact of Gold Nanoparticle Stabilizing Ligands on the Colloidal Catalytic Reduction of 4-Nitrophenol. *ACS Catal.* **2016**, *6*, 5553−5560.
(50) El Mhammedi, M. A.; Achak, M.; Bakasse, M.; Chtaini, A. Electrochemical Determination of Para-Nitrophenol at Apatite-Modified Carbon Paste Electrode: Application in River Water Samples. *J. Hazard. Mater.* **2009**, *163*, 323−328.
(51) Wang, P.; Xiao, J.; Liao, A.; Li, P.; Guo, M.; Xia, Y.; Li, Z.; Jiang, X.; Huang, W. Electrochemical Determination of 4-Nitrophenol Using Uniform Nanoparticle Film Electrode of Glass Carbon Fabricated Facilely by Square Wave Potential Pulses. *Electrochim. Acta* **2015**, *176*, 448−455.
(52) Liu, Z.; Ma, X.; Zhang, H.; Lu, W.; Ma, H.; Hou, S. Simultaneous Determination of Nitrophenol Isomers Based on β-Cyclodextrin Functionalized Reduced Graphene Oxide. *Electroanalysis* **2012**, *24*, 1178−1185.
(53) Liu, Z.; Du, J.; Qiu, C.; Huang, L.; Ma, H.; Shen, D.; Ding, Y. Electrochemical Sensor for Detection of P-Nitrophenol Based on Nanoporous Gold. *Electrochem. Commun.* **2009**, *11*, 1365−1368.
(54) Chu, L.; Han, L.; Zhang, X. Electrochemical Simultaneous Determination of Nitrophenol Isomers at Nano-Gold Modified Glassy Carbon Electrode. *J. Appl. Electrochem.* **2011**, *41*, 687−694.
(55) Xiao, G.; Zhao, Y.; Li, L.; Pratt, J. O.; Su, H.; Tan, T. Facile Synthesis of Dispersed Ag Nanoparticles on Chitosan-TiO2 Composites as Recyclable Nanocatalysts for 4-Nitrophenol Reduction. *Nanotechnology* **2018**, *29*, 155601.
(56) Da Cunha, G. C.; Dos Santos, B. T.; Alves, J. R.; Alves Silva, I. A.; De Souza Cruz, D. R.; Romao, L. P. C. Applications of Magnetic Hybrid Adsorbent Derived from Waste Biomass for the Removal of Metal Ions and Reduction of 4-Nitrophenol. *J. Environ. Manage.* **2018**, *213*, 236−246.
(57) Zhang, W.; Tan, F.; Wang, W.; Qiu, X.; Qiao, X.; Chen, J. Facile, Template-Free Synthesis of Silver Nanodendrites with High Catalytic Activity for the Reduction of p-Nitrophenol. *J. Hazard. Mater.* **2012**, *217-218*, 36−42.
(58) Zhu, X.; Shi, S.; Wei, J.; Lv, F.; Zhao, H.; Kong, J.; He, Q.; Ni, J. Electrochemical Oxidation Characteristics of P-Substituted Phenols Using a Boron-Doped Diamond Electrode. *Environ. Sci. Technol.* **2007**, *41*, 6541−6546.
(59) Di Paola, A.; Marcı, G.; Palmisano, L.; Schiavello, M.; Uosaki, K.; Ikeda, S.; Ohtani, B. Preparation of Polycrystalline TiO 2 Photocatalysts Impregnated with Various Transition Metal Ions : Characterization and Photocatalytic Activity for the Degradation Of. *J. Phys. Chem. B* **2002**, *106*, 637−645.
(60) Gkizis, P. L.; Stratakis, M.; Lykakis, I. N. Catalytic Activation of Hydrazine Hydrate by Gold Nanoparticles: Chemoselective Reduction of Nitro Compounds into Amines. *Catal. Commun.* **2013**, *36*, 48−51.
(61) Khan, M. U.; Siddiqui, Z. N. Halometallic Ionic Liquid Incorporated Graphene Nanosheets (IMD-Si/FeCl4−@GNS): A Highly Efficient Catalyst for the Reduction of 4-Nitrophenol and Nonenzymatic Glucose Sensing. *Curr. Res. Green Sustain. Chem.* **2021**, *4*, No. 100101.
(62) Khan, M. U.; Siddiqui, S.; Siddiqui, Z. N. Novel Ionic Liquid-Functionalized Chitosan [DSIM][AlCl 3] x- @CS: Synthesis, Characterization, and Catalytic Application for Preparation of Substituted Pyrazine Derivatives. *ACS Omega* **2019**, *4*, 7586−7595.
(63) Khan, M. U.; Rather, R. A.; Siddiqui, Z. N. Design, Characterization and Catalytic Evaluation of Halometallic Ionic Liquid Incorporated Nd2O3nanoparticles ([Smim][FeCl4]-@ Nd2O3) for the Synthesis of: N -Aryl Indeno Pyrrole Derivatives. *RSC Adv.* **2020**, *10*, 44892−44902.
(64) Rather, R. A.; Siddiqui, Z. N. Silver Phosphate Supported on Metal−Organic Framework (Ag3PO4@MOF-5) as a Novel Heterogeneous Catalyst for Green Synthesis of Indenoquinolinediones. *Appl. Organomet. Chem.* **2019**, *33*, 1−14.
(65) Shkrob, I. A.; Marin, T. W.; Bell, J. R.; Luo, H.; Dai, S. Radiation Stability of Cations in Ionic Liquids. 3. Guanidinium Cations. *J. Phys. Chem. B* **2013**, *117*, 14400−14407.
(66) Porras Gutiérrez, A. G.; Zeitouny, J.; Gomila, A.; Douziech, B.; Cosquer, N.; Conan, F.; Reinaud, O.; Hapiot, P.; Le Mest, Y.; Lagrost, C.; Le Poul, N. Insights into Water Coordination Associated with the CuII/CuIelectron Transfer at a Biomimetic Cu Centre. *Dalton Trans.* **2014**, *43*, 6436−6445.
(67) Chen, J.; Zhu, X. Ionic Liquid Coated Magnetic Core/Shell Fe3O4SiO2nanoparticles for the Separation/Analysis of Linuron in Food Samples. *Spectrochim. Acta A Mol. Biomol. Spectrosc.* **2015**, *137*, 456−462.
(68) Endo, T.; Masu, H.; Fujii, K.; Morita, T.; Seki, H.; Sen, S.; Nishikawa, K. Determination of Missing Crystal Structures in the 1-Alkyl-3- Methylimidazolium Hexafluorophosphate Series: Implications on Structure-Property Relationships. *Cryst. Growth Des.* **2013**, *13*, 5383−5390.
(69) Sabouni, R.; Kazemian, H.; Rohani, S. A Novel Combined Manufacturing Technique for Rapid Production of IRMOF-1 Using Ultrasound and Microwave Energies. *Chem. Eng. J.* **2010**, *165*, 966−973.
(70) Kumar, G.; Masram, D. T. Sustainable Synthesis of MOF-5@GO Nanocomposites for Efficient Removal of Rhodamine B from Water. *ACS Omega* **2021**, *6*, 9587−9599.
(71) Karimzadeh, Z.; Javanbakht, S.; Namazi, H. Carboxymethylcellulose/MOF-5/Graphene Oxide Bio-Nanocomposite as Antibacterial Drug Nanocarrier Agent. *BioImpacts* **2019**, *9*, 5−13.
(72) Yassin, F. A.; El Kady, F. Y.; Ahmed, H. S.; Mohamed, L. K.; Shaban, S. A.; Elfadaly, A. K. Highly Effective Ionic Liquids for Biodiesel Production from Waste Vegetable Oils. *Egypt. J. Pet.* **2015**, *24*, 103−111.

https://doi.org/10.1021/acsomega.2c05808
ACS Omega 2023, 8, 3785−3797

(73) Mustafa, A.; Siddiqui, Z. N. Silica-Based Ionic Liquid Supported on Xanthan [ImSi][PF6]@ Xanthan in the Synthesis of Acridine Derivatives by Multicomponent Reaction. *Sustain. Chem. Pharm.* **2022**, *29*, No. 100775.
(74) Tirmizi, S. A.; Badshah, A.; Ammad, H. M.; Jawad, M.; Abbas, S. M.; Rana, U. A.; Khan, S. U.-D. Synthesis of Highly Stable MOF-5@ MWCNTs Nanocomposite with Improved Hydrophobic Properties. *Arab. J. Chem.* **2018**, *11*, 26−33.
(75) Rodríguez, N. A.; Parra, R.; Grela, M. A. Structural Characterization, Optical Properties and Photocatalytic Activity of MOF-5 and Its Hydrolysis Products: Implications on Their Excitation Mechanism. *RSC Adv.* **2015**, *5*, 73112−73118.
(76) Shi, F.; Zhang, Q.; Li, D.; Deng, Y. Silica-Gel-Confined Ionic Liquids: A New Attempt for the Development of Supported Nanoliquid Catalysis. *Chem. - Eur. J.* **2005**, *11*, 5279−5288.
(77) Panja, S. K.; Srivastava, N.; Srivastava, J.; Prasad, N. E.; Noothalapati, H.; Shigeto, S.; Saha, S. Evidence of C−F-P and Aromatic π−F-P Weak Interactions in Imidazolium Ionic Liquids and Its Consequences. *Spectrochim. Acta A Mol. Biomol. Spectrosc.* **2018**, *194*, 117−125.
(78) Lyu, Q.; Yan, H.; Li, L.; Chen, Z.; Yao, H.; Nie, Y. Imidazolium Ionic Liquid Modified Graphene Oxide: As a Reinforcing Filler and Catalyst in Epoxy Resin. *Polymers (Basel)* **2017**, *9*, 447.
(79) Yan, Y.; Zhu, Y.; Zhang, L.; Zou, C.; Hu, Z.; Zhou, H.; Cai, L. Study on the Anodic Behavior of AISI E52100 Steel in Two Fluorine-Containing Ionic Liquids. *Res. Chem. Intermed.* **2021**, *47*, 2107−2123.
(80) Liu, X.; Pu, J.; Wang, L.; Xue, Q. Novel DLC/Ionic Liquid/Graphene Nanocomposite Coatings towards High-Vacuum Related Space Applications. *J. Mater. Chem. A* **2013**, *1*, 3797−3809.
(81) Peng, M. M.; Jeon, U. J.; Ganesh, M.; Aziz, A.; Vinodh, R.; Palanichamy, M.; Jang, H. T. Oxidation of Ethylbenzene Using Nickel Oxide Supported Metal Organic Framework Catalyst. *Bull. Korean Chem. Soc.* **2014**, *35*, 3213−3218.
(82) Zhang, H. Y.; Hao, X. P.; Mo, L. P.; Liu, S. S.; Zhang, W. B.; Zhang, Z. H. A Magnetic Metal−Organic Framework as a Highly Active Heterogeneous Catalyst for One-Pot Synthesis of 2-Substituted Alkyl and Aryl(Indolyl)Kojic Acid Derivatives. *New J. Chem.* **2017**, *41*, 7108−7115.
(83) Rafiee, E.; Joshaghani, M.; Eavani, S.; Rashidzadeh, S. A Revision for the Synthesis of β-Enaminones in Solvent Free Conditions: Efficacy of Different Supported Heteropoly Acids as Active and Reusable Catalysts. *Green Chem.* **2008**, *10*, 982−989.
(84) Ahmad, A. I.; El-Dafrawy, S. M.; Al-shorifi, F. T. Cobalt − Metal Organic Frameworks (Co-MOFs) Nanocatalyst: An Efficient Catalyst for the Preparation of 3,4-Dihydropyrimidinone. *Int. J. Nano Mater. Sci.* **2017**, *6*, 25−38.
(85) Chen, X.; Chen, X.; Cai, Z.; Oyama, M. AuPd Bimetallic Nanoparticles Decorated on Graphene Nanosheets: Their Green Synthesis, Growth Mechanism and High Catalytic Ability in 4-Nitrophenol Reduction. *J. Mater. Chem. A* **2014**, *2*, 5668−5674.
(86) Thawarkar, S. R.; Thombare, B.; Munde, B. S.; Khupse, N. D. Kinetic Investigation for the Catalytic Reduction of Nitrophenol Using Ionic Liquid Stabilized Gold Nanoparticles. *RSC Adv.* **2018**, *8*, 38384−38390.
(87) Pachfule, P.; Kandambeth, S.; Díaz, D. D.; Banerjee, R. Highly Stable Covalent Organic Framework−Au Nanoparticles Hybrids for Enhanced Activity for Nitrophenol Reduction. *Chem. Commun.* **2014**, *50*, 3169−3172.
(88) Li, J.; Liu, C.; Liu, Y. Au/Graphene Hydrogel: Synthesis, Characterization and Its Use for Catalytic Reduction of 4-Nitrophenol. *J. Mater. Chem.* **2012**, *22*, 8426−8430.
(89) Bendi, R.; Imae, T. Renewable Catalyst with Cu Nanoparticles Embedded into Cellulose Nano-Fiber Film. *RSC Adv.* **2013**, *3*, 16279−16282.
(90) Zhang, P.; Shao, C.; Zhang, Z.; Zhang, M.; Mu, J.; Guo, Z.; Liu, Y. In Situ Assembly of Well-Dispersed Ag Nanoparticles (AgNPs) on Electrospun Carbon Nanofibers (CNFs) for Catalytic Reduction of 4-Nitrophenol. *Nanoscale* **2011**, *3*, 3357−3363.
(91) Pradhan, N.; Pal, A.; Pal, T. Catalytic Reduction of Aromatic Nitro Compounds by Coinage Metal Nanoparticles. *Langmuir* **2001**, *17*, 1800−1802.
(92) Corma, A.; Concepción, P.; Serna, P. A Different Reaction Pathway for the Reduction of Aromatic Nitro Compounds on Gold Catalysts. *Angew. Chem., Int. Ed.* **2007**, *46*, 7266−7269.
(93) Rong, J.; Qiu, F.; Zhang, T.; Zhu, Y.; Xu, J.; Guo, Q.; Peng, X. Non-Noble Metal@carbon Nanosheet Derived from Exfoliated MOF Crystal as Highly Reactive and Stable Heterogeneous Catalyst. *Appl. Surf. Sci.* **2018**, *447*, 222−234.
(94) Du, C.; Gao, Y.; Wang, J.*Achieving 59% Faradaic Efficiency of N2 Electroreduction Reaction in Aqueous Zn-N2 Battery by Facilely Regulating the Surface Mass Transport on Metallic Copper*. *Chem. Commun.*201955, 12801−12804, DOI: 10.1039/C9CC05978D.
(95) Zhang, Y.; Qiu, W.; Ma, Y.; Luo, Y.; Tian, Z.; Cui, G.; Xie, F.; Chen, L.; Li, T.; Sun, X. High-Performance Electrohydrogenation of N2 to NH3 Catalyzed by Multishelled Hollow Cr2O3 Microspheres under Ambient Conditions. *ACS Catal.* **2018**, *8*, 8540−8544.

https://doi.org/10.1021/acsomega.2c05808
ACS Omega 2023, 8, 3785−3797